High-Frequency Surface Wave Radars in the Mediterranean Sea: civil and environmental applications

Charles-Antoine Guérin, Milan Rozel, Dylan Dumas, Michel Menelle, Veronica Morales-Marquez, Laurent Perus

High-Frequency Surface Wave Radars in the Mediterranean Sea: civil and environmental applications

1st Charles-Antoine Guérin
MIO (Univ. Toulon, Aix-Marseille Univ., CNRS, IRD)
Université de Toulon
Toulon, France
guerin@univ-tln.fr

2nd Milan Rozel
DEMR
ONERA, Université Paris-Saclay
91120, Palaiseau, France
milan.rozel@onera.fr

3rd Dylan Dumas
MIO
CNRS
Toulon, France
dylan.dumas@mio.osupytheas.fr

4th Michel Menelle
DEMR
ONERA, Université Paris-Saclay
91120, Palaiseau, France
michel.menelle@onera.fr

5th Veronica Morales-Marquez
MIO
Université de Toulon
Toulon, France
veronica.morales-marquez@mio.osupytheas.fr

6th Laurent Perus
DEMR
ONERA, Université Paris-Saclay
91120, Palaiseau, France
laurent.perus@onera.fr

***Abstract*—The Mediterranean Institute of Oceanography (MIO) has been operating for one decade a network of high-frequency radars for the monitoring of coastal surface currents on the French Mediterranean coast. More recently, ONERA has been developing an original over-the-horizon radar system for the detection and tracking of ships in the coastal zone. The two institutions have joined their efforts to provide dual civil and environmental applications of surface wave radars in the framework of the ROSMED project. We present preliminary results of the unique capabilities of the ONERA radar for the mapping of surface currents at very long range in the Gulf of Lion. We also present new results of the MIO high-frequency radar for the measurement of surface currents and waves and the automatic detection of ships.**

***Index Terms*—High-Frequency Surface Wave Radar, ocean surface current, ocean waves, ship detection.**

I. Introduction

High-Frequency Surface Wave Radars (HFSWR) have been in use for a long time for the monitoring of coastal areas, both for environmental and civil applications ([1]–[4]). The number of HFSWR stations has increased considerably in recent years and today there are more than 400 of these instruments deployed worldwide [5]. Recently, the only two institutions operating HFSWR on the French Mediterranean coast, namely the Mediterranean Institute of Oceanography (MIO) and the French Aerospace Lab (ONERA) have joined forces in a joint project* to share their experience in the field of oceanography and ship detection, respectively.

II. The ONERA HFSWRs

For over two decades, ONERA has been developing HF-SWRs for long-range ship target detection. It started with a classical pulsed phased array radar in the early 2000's, with limited azimuthal resolution being the main weakness of the architecture [6]. It has evolved to a synthetic array with MIMO waveforms, which allowed improved azimuthal resolution with a small number of antennas over a large baseline [7]. Since 2020, the MIMO concept has been continued with a third-generation system with an increased number of transmit and receive antennas, allowing a further increase in range and resolution. This latest HFSWR system is called ROS NG ("Radar à Ondes de Surface de Nouvelle Génération") and is currently operated in salt ponds on the southern coast of France (see Figure 1).

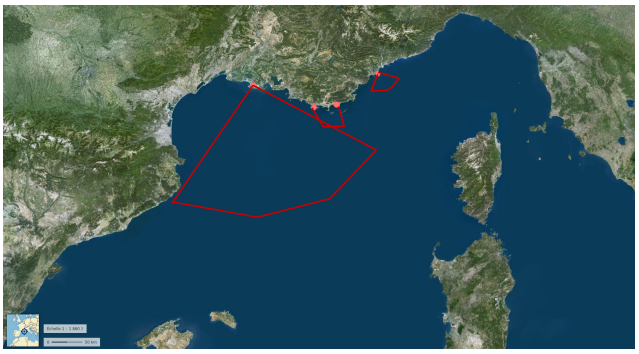

Fig. 1. Location of the 3 HFSWRR networks on the French Mediterranean frontside together with their approximate spatial coverage. The ONERA operates a single station in Aigues-Mortes as of 2024; the MIO operates 2 WERA® stations in the region of Toulon and onde SeaSonde® station in Nice.

It is mounted in a quasi-monostatic configuration with 18 transmit antennas and 32 receive antennas, resulting in a 2D synthetic antenna array. All the antennas are placed in

*Part of this research and one of the authors (VMM) have been funded by the Agence Nationale de la Recherche (ANR) under grant ANR-22-ASTR-0006-01 (ROSMED project: "Radar à Ondes de Surface en MEDiterranée").

the water of the salt pond, which ensures an almost perfect adaptation of the antennas to the propagation medium and greatly increases the antenna gain for surface wave operations. The RX array is a linear array of 32 antennas consisting of four disjoint subarrays of eight antennas each (see Figure 2). The TX array is a broad-fire array consisting of three end-fire subarrays. After synthetic antenna processing, it becomes a virtual 2D array that acts as both an end-fire and a broad-fire array at the same time, as the array's antennas are both perpendicular and parallel to the aiming direction. This architecture provides beamforming capability in both azimuth and elevation. This prototype is intended to evaluate this original HFSWR architecture and demonstrate its performance. The primary function of this system is the detection of ships off the French Mediterranean coast but, it can and will also be used for oceanographic measurements.

A. Experimental set-up

The preliminary results presented in this study do not take the full capabilities of the ROS NG. In this first experiment, we used only eight physical RX antennas have and only one TX antenna without synthetic antenna processing. The transmitted power is therefore much lower than that of the future operational system. The experiment was performed with a transmit power of 50 W at a center frequency of $f_0 = 6.5$ MHz and a transmit bandwidth of 50 kHz, resulting in a theoretical range resolution of 3 km. The transmitted waveform consists of ascending chirps with a PRF of 100 Hz.

Fig. 2. Two of the four RX sub-arrays of the ROS NG in the salt pond of Aigues-Mortes.

B. First results

A series of tests were performed over 3800 seconds using a single TX antenna and the 4 physical sub-arrays of 8 RX antennas. Figure 3 shows a range-Doppler map obtained with these data, integrated over 300 seconds, the Bragg lines are clearly visible out to 100km. Due to heavy sea conditions on that day and the absence of maritime traffic in the range of the radar at the time of recording, this measurement was not appropriate to test ship detection. However, it could be used for oceanographic purposes using the same methodology as described in Section III-B. Figure 4 shows the first radial current map derived from the available record of ROS NG data. The classic patterns of oceanic circulation can be seen on this map, with visible dipole structures corresponding to the radial projection of eddies and a sharp current front extending along the northeast-southwest axis.

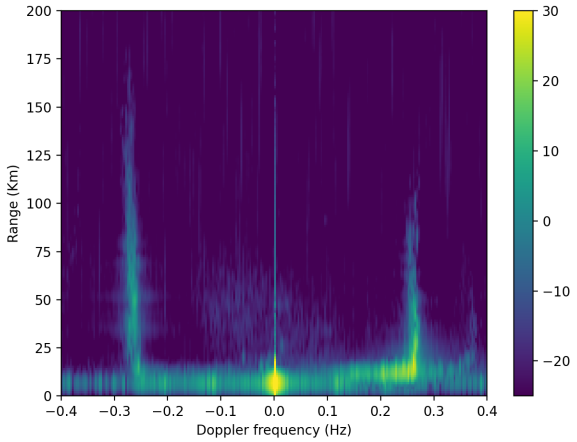

Fig. 3. Range-Doppler map obtained from the ROS NG data with 5 minutes integration time. The power is not calibrated.

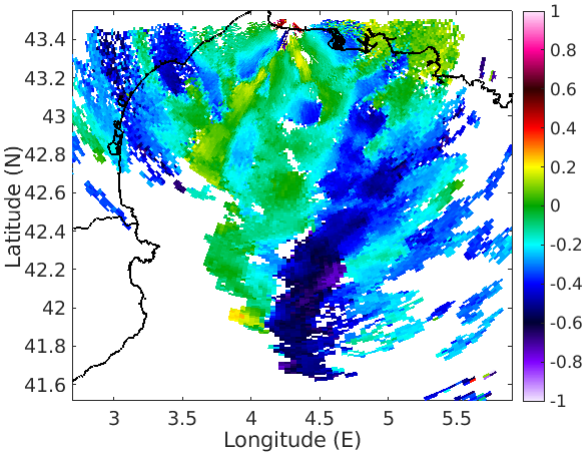

Fig. 4. First map of radial currents (given in m/s) measured by the ROS NG in the Gulf of Lion with 1 TX and an RX array of eight antennas over 1 hour. Even in this reduced configuration, the useful radar coverage extends to about 200 km offshore.

III. The MIO HFSWR network

A. Radar sites and instruments

The Mediterranean Institute of Oceanography, with the support of the Centre National de la Recherche Scientifique (CNRS) and the University of Toulon, has developed a network of oceanographic HFSWR for more than ten years to observe the coastal maritime zone between Toulon and Nice. The first part of this network consists of 2 transmitters and 2 receivers of WERA® phased-array radars manufactured by Helzel GmbH[1], which are located at 3 remote sites in the Toulon area and operating in multistatic mode [8], [9].

[1]https://helzel.com/

An additional HFSWR monostatic system is located near Nice [10], at the lighthouse of Saint-Jean Cap Ferrat. It is a SeaSonde® radar manufactured by CODAR Ocean Sensors[2], which uses a compact antenna system. The primary oceanographic application of these instruments is the continuous, near real-time measurement of ocean surface currents, with integration times of the order of an hour. The WERA and CODAR HFSWR operate in the High Frequency (HF) band at a central frequency of 16.15 MHz and 13.5 MHz, respectively, with an assigned bandwidth of 100 kHz. The typical range of these instruments is on the order of 60 km, depending on the meteorological conditions, with a range resolution of 1.5 km.

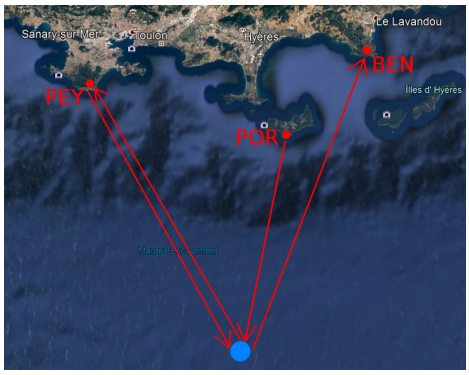

Fig. 5. The HFR network in the region of Toulon is composed of a TX-RX at Fort Peyras (PEY), a stand-alone RX at the Cap Bénat (BEN) and a stand-alone TX at Porquerolles (POR).

B. Measuring the surface currents

Each radar receiver measures a component of the surface current vector in each radar cell that can be resolved on the sea surface. In the monostatic geometry, this component is the radial projection in the direction of the radar; in the bistatic geometry, i.e. when the transmitter is far away from the receiver, it is an elliptical projection on the TX-RX axis. By combining the projections measured by two different stations onto their common spatial footprint, one can reconstruct the current vector. This is done with the Toulon network, in which the monostatic TX-RX pair Peyras-Peyras is combined with the bistatic TX-RX pair Porquerolles-Bénat, see Figure 5. For the SeaSonde system at Nice, only one radial projection of the surface current is available. High-resolution extraction and mapping of radial or elliptical ocean currents from radar data requires a complex signal processing chain. The first processing steps, which are common to phased-array and compact antenna systems, are quite standard: they include the generation of the demodulated I & Q signal with 2 mixers, the range binning of the signal with the classical FMCW technique and the generation of the complex Doppler spectra with a Fast Fourier Transform with appropriate integration time. A further step is the azimuthal processing, which is usually performed with the Beam Forming (BF) technique for phased arrays and with high-resolution Direction Finding (DF) methods for compact antennas. These two methods have different advantages and shortcomings. The BF is simple to apply and robust to noise; it allows the calculation of directional Doppler spectra that can be used for wave inversion or ship detection. However, its azimuthal resolution is limited by the length of the array and degrades at large angles of view from the array axis (it is generally restricted to an angular sector of ± 60 degrees around the normal). The DF method, which is based on the MUSIC algorithm, allows in principle a higher azimuthal resolution but is more difficult to use as it requires a certain number of parameters to be optimized and because it is plagued with wrongly assigned surface current directions and outliers; it requires a longer integration time and produces lacunar surface current maps. Recently, the DF technique has been adapted to phased arrays and improved to provide full spatial coverage of the surface current map, to mitigate the influence of noise, and to eliminate the errors [11], [12]. This allows the production of high-quality hourly maps in near real-time (see hfradar.univ-tln.fr). Figure 6 shows an example of 2 radial maps simultaneously measured by the 2 WERA receivers at Peyras and Bénat, together with the reconstructed surface current field.

[2]https://codar.com/

C. Measuring waves

This work expands the oceanographic applications of HF Radar to include the estimation of significant wave height (H_s) as well as the peak period (T_p) of dominant waves. Characteristics of the wave field are derived from Doppler spectra using the classical theory outlined by [13]. This approach is based on a complex theoretical formulation, wherein the H_s is estimated from the ratio of the weighted integral of the second-order Doppler spectrum to the energy of the first-order peaks, known as Bragg lines.

$$H_s^2 = \frac{32 \int_{-\infty}^{\infty} \sigma_2(\omega)/w(_{\omega/\omega_B})d\omega}{k_0^2 \int_{-\infty}^{\infty} \sigma_1(\omega)d\omega}, \tag{1}$$

where σ_1 and σ_2 are the first-order and second-order Doppler spectrum, w is the weighted function defined in [13] and k_0 scalar radio wavenumber. The period of the dominant waves can also be determined from a different ratio of integrals that relies solely on the second-order Doppler spectrum.

$$T_p = \frac{\int_{0,\omega_B}^{\omega_B,\infty} \sigma_2(\omega)/w(_{\omega/\omega_B})d\omega}{\int_{0,\omega_B}^{\omega_B,\infty} |\omega - \omega_B|\sigma_2(\omega)/w(_{\omega/\omega_B})d\omega} \tag{2}$$

The main challenge of this methodology is the effective differentiation between first- and second-order spectra, along with the precise distinction of signal versus noise. To overcome this, specific techniques have been developed that allow for the accurate setting of separation thresholds and the establishment of control criteria for integration areas. This technique's effectiveness is limited by its dependence on the second-order Doppler spectrum, restricting its application to shorter distances where this spectrum remains significantly above the noise level. This method is used with radar signal data both omnidirectional (signal collected before performing

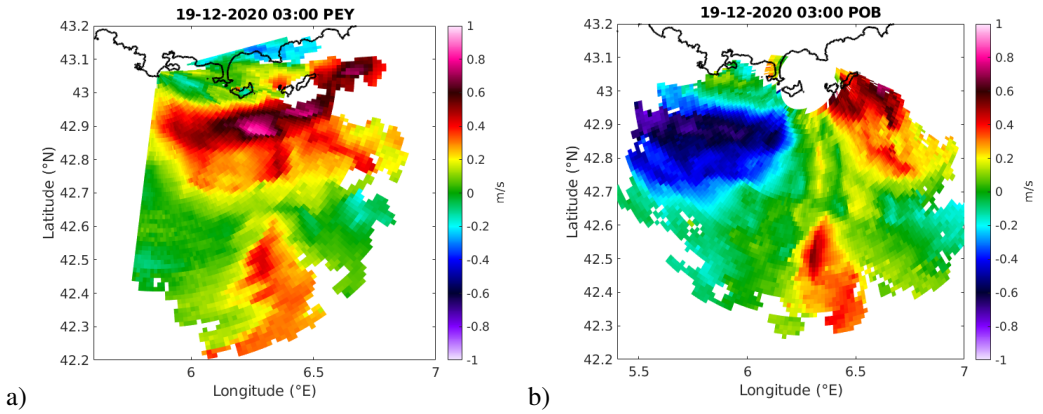

Fig. 6. Hourly radial surface current measured on 19 December 03:00 UTC, 2020, with the HFSWR stations of a) Peyras; b) Bénat.

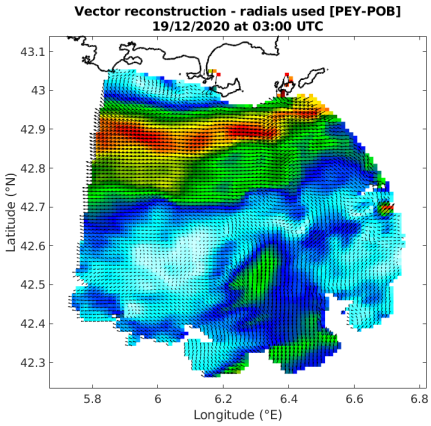

Fig. 7. Total surface current reconstructed from the radials on Figure 6

the beamforming method) and directional (signal observed after applying the beamforming method). The big difference between these two data sets is that with the omnidirectional signal, we cannot distinguish the precise azimuth from where the signal comes from, therefore we have the signal sorted only by ranges (distance to the radar), while applying the beamforming method, we can distinguish both range and azimuth from where we receive the signal. The results obtained for H_s and T_p for the whole year 2020 using only the data from the Fort Peyras station are shown in Fig. 8. There, we can see that the results obtained with the radar using the [13] method fit quite well with the data collected by the Candhis buoy located in the vicinity of Porquerolles. Specifically, we have obtained an average Pearson correlation coefficient and an average Root Mean Square Error (RMSE) between the directional H_s data from the radar and the buoy (from here on, all the static values mentioned have been calculated taking as reference the H_s and T_p variables of the Candhis buoy of Porquerolles) of 76% and 0.64m, respectively, finding the maximum of correlation of 89% and the minimum of RMSE around 0.39m in the center of the radar domain. As for the results obtained with the omnidirectional signal, we have an average correlation coefficient of 81% and an average RMSE of 0.61m, with a maximum correlation coefficient of 87% and a minimum RMSE of 0.43m. More details can be found in [14]. Regarding the results obtained for the T_p, we can observe in Fig. 8b and 8d, how the accuracy is slightly lower. This could be because the calculation of T_p is much more sensitive to the differentiation between the signal and the noise, as we use second-order spectra (Eq. 2). Thus, we obtain an average correlation value of 47%, both directional and omnidirectional T_p, and an average RMSE of 1.42s and 1.37s (in directional and omnidirectional respectively), while we find maximum correlation values around 60% in directional T_p and 54% in omnidirectional T_p, and a minimum RMSE of 1.26s and 1.30s (directional and omnidirectional respectively) in the center of the radar domain. As we can observe, the results obtained with the omnidirectional signal can provide an accurate approximation of the wave features in the study area. However, we do not have azimuthal resolution to know from which direction specifically that wave is coming, since we consider that for all azimuths within the same range, the wave has the same characteristics. The method limitations are visible in Fig. 8, where we can see that the farther we are from the radar (Fig. 8c and 8d) the more inaccurate the radar results (red and green lines) are with respect to the Candhis buoy data (blue line).

D. Ship detection

Ship detection is based on the identification of bright spots in the Range-Doppler spectra. Ships traveling with their typical speed under the radar coverage will cross a radar resolution cell within a few minutes. Therefore, they must be observed with a shorter integration time than is usually used for surface currents. For this purpose, a series of "short" Doppler spectra are processed over each hour of observation time; these are referred to as "instantaneous Doppler spectra" to distinguish them from the background Doppler spectra, which are averaged over a longer period (typically, one hour, a period over which the ocean parameters are assumed to be stationary) for the estimation of the radial surface currents and waves. Because the oceanic features in the range-Doppler maps, such

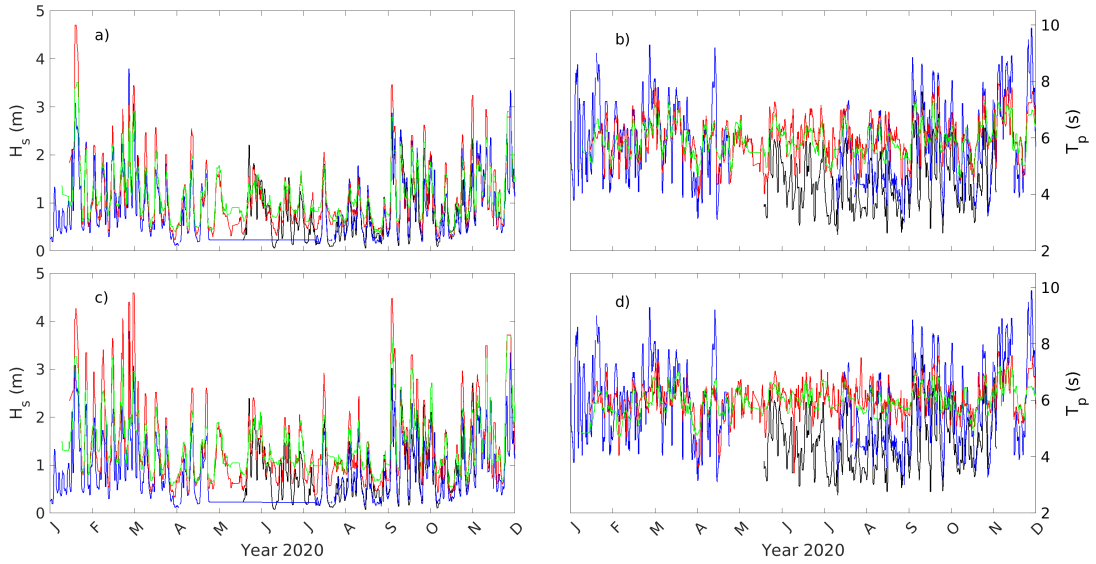

Fig. 8. Time series of H_s (a, c) in meters and T_p (b, d) in seconds at different radar distances in azimuth 75 (in the center of radar coverage). a, b) are measured at 15km, c,d) at 22.5km from the radar. The blue line represents the data from the Candhis buoy located at Porquerolles, the black line is the result of the WaveWatch III model run in the area, green and red lines are the results obtained after using the omnidirectional and direction HF radar data with the method of [13].

as the first- and second-order Bragg lines, change slowly, ships can be distinguished from the latter by strongly contrasting instantaneous Doppler spectra with respect to the background spectra in a given range-frequency cell. To eliminate the contribution of ships in the calculation of the background spectra, the latter are obtained by taking the median of the former over one hour. Since a ship in motion does not occupy the same range-Doppler cell for such a long time, its strong echo, which addresses only a few instantaneous Doppler spectra, is eliminated in this process. We now detail the precise algorithm that leads to reliable ship detection. Directional instantaneous Doppler spectra are obtained by processing the range-sorted radar data in azimuth (using the BF technique) and frequency (using a windowed Fourier Transform). For this purpose, short portions of the time series are selected with overlapping Blackman windows of 2 minutes which are shifted by 1/5 of their length at each update time. The resulting Doppler spectra $S_{inst}(R, \theta, f, t)$ depend on the range R, the azimuth θ, the Doppler frequency f, and the update time t. The background Doppler spectra are obtained by taking the median of the instantaneous spectra over time:

$$S_{background}(R, \theta, f) = \text{median}_t S_{inst}(R, \theta, f, t) \qquad (3)$$

To reduce noise variance, which can result in bright spots that can be confused with ships in the Range-Doppler representation, the instantaneous and background Doppler spectra are smoothed with a running average over a few neighboring range-frequency cells (typically, the 2 or four adjacent bins) and a few successive time steps. The instantaneous noise floor $N(R, \theta, t)$ is estimated by taking the median of the Doppler spectra over frequencies (because more than 50% in the 4 Herz bandwidth is occupied by noise):

$$N(R, \theta, t) = \text{median}_f S_{inst}(R, \theta, t) \qquad (4)$$

The four-dimensional cells (R, θ, f, t) corresponding to a ship can be distinguished from noise by imposing a minimum value above the noise floor (where the values are taken in dB)

$$(S_{inst}(R, \theta, f, t))_{dB} > (N(R, \theta, t))_{dB} + T, \qquad (5)$$

for some threshold T that must be empirically fixed (here, $T =$ 12 dB). The four-dimensional cells (R, θ, f, t) that correspond to a ship can be distinguished from the oceanic features by imposing a minimum value above the background level:

$$(S_{inst}(R, \theta, f, t))_{dB} > (S_{background}(R, \theta, f))_{dB} + T \qquad (6)$$

Only the cells that satisfy the simultaneous conditions (5) and (6) are retained for the ships (Figure 9c).) The exact positions of the ships at time t are obtained by finding the local maxima of the remaining cells for the (R, θ, f) variables. A barycenter of each variable R, θ, and f with respect to the instantaneous Doppler spectrum is performed in the neighborhood of these local maxima to refine the estimate.

Examples of instantaneous and background Doppler spectra, as described in steps 1 and 2 above, are shown in Figure 9 in the range-Doppler representation. Also shown are the retained cells for ship localization after applying steps 5 and 6 above. The application of this algorithm over a full day of radar data is shown in Figure 10. The radar-based estimates of the ship coordinates are compared with Automatic Identification System (AIS) records of the cooperative vessels. The AIS receptor was developed and supplied by eOdyn (https://www.eodyn.com/). At this stage of preliminary results, the detection performance has not yet been established.

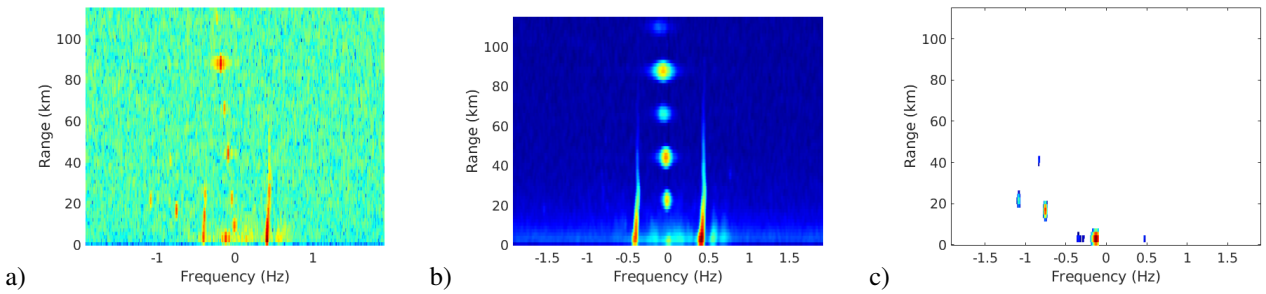

Fig. 9. Examples of a) instantaneous and b) background Doppler spectra measured on June 15, 2023, at the Fort Peyras HFSWR station. The bright red spots close to the zero-Doppler vertical line are artifacts of the power grid instability. The first-order Bragg lines are visible up to about 70 km away and the second-order sidebands of the ocean Doppler spectrum can be seen up to 15-20 km away. These oceanic features as well as the background noise are eliminated by the various masks (steps 5 and 6 of the detection algorithm), thus revealing the remaining ship contribution (c).

However, a simple visual inspection shows an excellent overall agreement between the radar and AIS estimates. Note that there are a few obvious trajectories in the radar detection with no corresponding AIS records. This indicates the presence of some non-cooperative vessels.

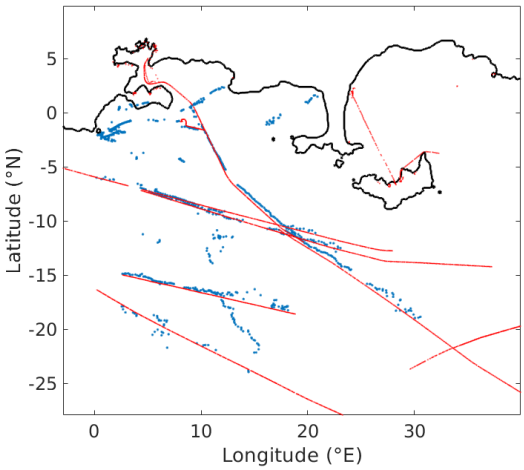

Fig. 10. Ship detection in the coastal area of Toulon on June 15, 2023. The red lines show the trajectory of cooperative ships equipped with AIS. The blue symbols show the positions of the ships detected with the HFSWR of Fort Peyras with an update time of about 1 minute.

IV. Conclusion

Dual applications of the ONERA and MIO HFSWR on the French Mediterranean coast have been presented and show promising results. Further results and performances will be presented at the conference.

Acknowledgment

We acknowledge the MOOSE program (Mediterranean Ocean Observing System for the Environment) coordinated by CNRS-INSU and the Research Infrastructure ILICO (CNRS-IFREMER). We are grateful to the Parc National de Port-Cros (PNPC) for its support and hosting of our radar transmitter in Porquerolles Island. We are also grateful to the "Association Syndicale des Propriétaires du Cap Bénat" (ASPCB) for hosting our receiver array at the Cap Bénat as well as the Group Military Conservation and the Marine Nationale for hosting our radar installation in Fort Peyras. Thanks to Clément Le Goff of eOdyn for providing the AIS data in Fort Peyras.

References

[1] J.D. Paduan and L. Washburn. High-Frequency radar observations of ocean surface currents. *Annual review of marine science*, 5:115–136, 2013. Publisher: Annual Reviews.

[2] L R Wyatt and others. HF radar: Applications in coastal monitoring, planning and engineering. In *Coasts and Ports 2013: 21st Australasian Coastal and Ocean Engineering Conference and the 14th Australasian Port and Harbour Conference*, page 878. Engineers Australia, 2013.

[3] E. Reyes et al. Coastal High-Frequency radars in the Mediterranean - Part 2: Applications in support of science priorities and societal needs. *Ocean Science*, 18:797–837, 2022.

[4] L. Pablo et al. Coastal High-Frequency radars in the Mediterranean - Part 1: Status of operations and a framework for future development. *Ocean Science*, 18:761–795, 2022.

[5] H. Roarty et al. The global High-Frequency radar network. *Frontiers in Marine Science*, 6:164, 2019. Publisher: Frontiers.

[6] M. Menelle and F. Jangal. Performance of surface wave radar based on frequency range. In *OCOSS2010, Brest*. SEE, 2010.

[7] F. Jangal and M. Menelle. French HFSWR contribution to the European integrated maritime surveillance system I2C. In *IET International Radar Conference 2015*, pages 1–5, 2015.

[8] C.-A. Guérin, D. Dumas, A. Gramoullé, C. Quentin, M. Saillard, and A. Molcard. The multistatic HF radar network in Toulon. In *IEEE Radar 2019 Conference*. IEEE, 2019.

[9] D. Dumas, A. Gramoullé, C.-A. Guérin, A. Molcard, Y. Ourmieres, and B. Zakardjian. Multistatic estimation of High-Frequency radar surface currents in the region of Toulon. *Ocean Dynamics*, 70(12):1485–1503, 2020. Publisher: Springer.

[10] C.-A. Guérin et al. High-frequency radar measurements with codar in the region of nice: Improved calibration and performance. *Journal of Atmospheric and Oceanic Technology*, 38(11):2003 – 2016, 2021.

[11] D. Dumas and C.-A. Guérin. New signal processing techniques for phased-array oceanographic radars: self-calibration, antenna grouping, and de noising. *Journal of Atmospheric and Oceanic Technology*, 40(6):753 – 769, 2023.

[12] D. Dumas, A.C. Bennis, C.-A. Guérin, G. Lopez, and M. Boutet. High-Frequency radar observation of strong and contrasted currents: the Alderney race paradigm. *ArXiv*, 2024. https://doi.org/10.48550/arXiv.2407.03827.

[13] D.E. Barrick. Extraction of wave parameters from measured HF radar sea-echo Doppler spectra. *Radio Science*, 12(3):415–424, 1977. Publisher: AGU.

[14] V. Morales-Márquez, D. Dumas, and C.-A. Guérin. HF radar estimation of ocean wave parameters: second-order Doppler spectrum versus Bragg wave modulation approach, 2024. *ArXiv*, 2024. https://doi.org/10.48550/arXiv.2407.07658.